J Biorheol (2014) 28:55–60
DOI 10.17106/jbr.28.55

BRIEF COMMUNICATION

Orientation transition of defective lyotropic triblock copolymer lamellar phase

Shuji Fujii[1,*], Yuuki Yamamoto[1]

[1]*Department of Chemistry, Nagaoka University of Technology, Niigata 940-2188, Japan*

Received: 9 October 2013 / Accepted: 1 May 2014 / Published online: 14 November 2014

Abstract We study concentration dependence of the critical shear rate of a layer orientation transition in lyotropic triblock copolymer lamellar phase. Theory predicts that suppression of undulation fluctuation by shear triggers the transition. The critical shear rate at high polymer concentration is in reasonable agreement with theory. However, experimental results at low polymer concentrations show different behavior from the prediction. Violation of the theory is attributed to defective nature of the lamellar phase, in which creation of defects prevents the suppression of the undulation fluctuation.

1. Introduction

Layered systems such as amphiphilic lamellar phases and thermotropic smectic phases often show fascinating non-equilibrium phase transition under shear [1–12]. Weak shear flow usually aligns layers in *c*-orientation, where the layer normal is parallel to the velocity gradient (∇v) direction (see Fig. 1). Once shear rate exceeds over a critical value, drastic change of the orientation is induced. In the layered system, two non-equilibrium structural transitions are observed. One is a shear-induced onion phase reported for many kinds of lyotropic lamellar phases [1–5, 9]. The other is layer orientation transition from *c* to *a*-orientation, which is generally appeared at high shear rate region [1, 3–5, 12]. Here, *a*-orientation corresponds to perpendicular orientation, where the layer normal is parallel to the neutral direction (*n*). In some lamellar systems, both structural transitions are induced as a function of shear rate [1, 3–5]. Main issue in the rheology of the layered systems is to find out what mechanism causes the non-equilibrium phase transition and how the specific non-equilibrium structure is chosen among these two alternatives. Knowledge on the non-equilibrium phenomena of the lamellar phase can be extended into many applications, including a biorheological problem such as a rheology of a thrombocyte in a blood flow.

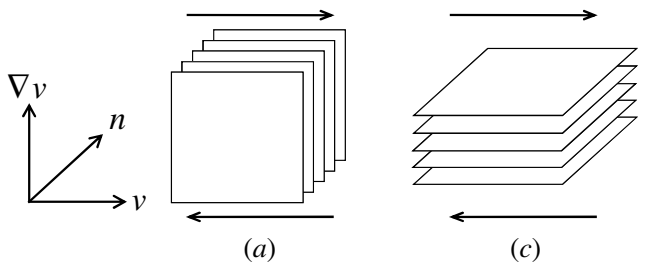

Fig. 1 Schematic diagram of the lamellar phase with (*a*) perpendicular and (*c*) parallel orientations. ∇v, v and n respectively correspond to the velocity gradient, flow and neutral directions.

*E-mail: sfujii@mst.nagaokaut.ac.jp

Instability of the lamellar phase is explained by the Helfrich-Hurault mechanism [13–17]. The Helfrich-Hurault effect is undulation instability of the smectic phase subjected to the external electric or magnetic field [17]. In the thermal equilibrium state, the undulation fluctuation yields repulsive Helfrich interaction between membranes which stabilizes the lamellar phase [18]. Suppression of the undulation fluctuation by shearing will reduce the repulsive force and destabilize lamellar membranes which causes the reduction of layer spacing. Thus reduced repulsive force generates effective dilation along the layer normal of the membrane in order to retain the equilibrium layer spacing. It has been anticipated that, as the dilation becomes larger than the critical value, coherent buckling of the lamellar membranes appears and either the onion phase formation or the layer orientation is eventually triggered [13–16]. However, experimental observations present that the onion phase formation and the layer orientation transition occur in different shear rate range [1, 4, 5]. Applying only one mechanism, the Helfrich interaction, into different struc-

tural transitions with different time scale is unreasonable. One possibility to clarify the difference between two structural transitions is to introduce the role of defects on the instability. Oswald et al. proposed that defects generated from flowing smectic in misaligned plates also induce the dilation strain [19]. Wunenburger and co-workers extended this idea and demonstrated that the shear induces destabilization in the flow direction [15]. We have also recently presented that the defect formation is essential for the shear-induced onion formation [10]. It is of great importance to revisit in the shear-induced structural transition from the viewpoint of defect-mediated rheology. Especially on the layer orientation transition, the role of defects has never been mentioned so far.

In this study, we examine dynamic orientation state of the lyotropic lamellar phase under shear by means of rheometry, birefringence, and small angle scattering methods. In the Helfrich stabilized system, the critical shear rate of the layer orientation transition follows scaling behavior of $\dot{\gamma} \sim \eta^{-1} d^{-3}$ [13, 20, 21], where η_0 and d are respectively the zero-shear viscosity and layer spacing. We will show that the critical shear rate of the layer orientation transition for the sample with fewer defects is comparable to the theoretical prediction. On the contrary, the defective lamellar phase shows different behavior from the prediction. The violation of the theoretical prediction in the defective lamellar phase is the first observation. The defect significantly contributes to the non- equilibrium structural transition.

2. Experimental

We used ternary lyotropic lamellar phase composed of amphiphilic triblock copolymer, Butanol, and distilled water. The amphiphilic triblock copolymer, trade name of Pluronic P123, was obtained from BASF and used as received. Pluronic P123 consists of two hydrophilic ethylene oxide, EO, blocks bounded to a central hydrophobic propylene oxide, PO, block. Hydrophilic EO chains at both sides have an identical chain length. Degree of polymerization of PO and EO blocks are $N_{PO} \approx 70$ and $N_{EO} \approx 20$, respectively. Prescribed amount of block copolymer and Butanol were dissolved into the distilled water H_2O and stirred for 2 days. In this study, the solvent composition, the ratio of butanol against the water B/H, was fixed at 0.3. And Pluronic P123 concentration was varied in the range of 20–30 wt%. The stable lamellar phase can be obtained only within the limited concentration range [4].

Viscosity measurement was performed using an ARES-G2 strain-controlled rheometer of TA Instrument Co., Ltd., with a couette geometry (hight of bob; 13 mm, gap size; 250 μm). Depolarized small angle light scattering measurement under shear (Rheo-SALS) was performed by using a stress controlled rheometer, Anton Paar MCR- 301, equipped with plate/plate shear geometry made of quartz. Gap size between plates was fixed at 250 μm which corresponds to the viscosity measurement. The incident beam of He-Ne laser (λ = 658 nm) was polarized along to the flow direction and the analyzer was aligned perpendicular to the flow direction. SALS pattern projected on the screen was recorded by CCD camera. In birefringence measurement under shear, He-Ne laser (λ = 633 nm) was incident on the sample along the velocity gradient direction and transmitted light was detected by the photodiode. Rheo-SAXS experiments were also performed using synchrotron radiation at beam line BL-10C of the Photon Factory at the Institute of Materials Structure Science of the High Energy Accelerator Research Organization in Tsukuba, Japan [22]. Self-made shear cell with couette geometry, which has the gap of 1 mm, was equipped on the beam line. In the rheo-SAXS measurements, two scattering configurations: (i) radial and (ii) tangential, were used. In the radial configuration, beam passes the sample along the velocity gradient direction so that the scattering pattern in the flow-neutral plane is obtained. In the tangential one, on the other hand, the beam passes along the flow direction. Thus, the scattering pattern in the velocity gradient-neutral plane is obtained. All measurements were performed at T = 25°C.

3. Results and Discussion

Figure 2 shows the viscosity η and birefringence $|\Delta n|$ as a function of the shear rate for samples with polymer concentration of (a): c = 20 wt% and (b): 24 wt%. In the bottom, rheo-SALS patterns at several shear rates are shown. In Fig. 2(a), after the Newtonian behavior at low shear rate, slight shear-thickening was observed at $\dot{\gamma} = 3s^{-1}$. As the shear rate was increased, the shear-thickening shifted to shear-thinning behavior. At high shear rate, the second Newtonian appeared and followed by the second shear-thinning at high shear rate. In Fig. 2(b), on the other hand, the Newtonian was followed by the shear-thinning behavior. Further increase in the shear rate induced the shear-thickening behavior at $\dot{\gamma} = 150s^{-1}$. At high shear rate, the second shear-thinning appeared. Zero-shear viscosity at c = 20 wt% was higher than that at c = 24 wt% while both showed a similar value in the second shear-thinning.

Birefringence also showed clear difference between these systems. In Fig. 2(a), $|\Delta n|$ was decreased as the shear-thickening appeared and turned to the increase with the shear rate in the shear-thinning region. In the second Newtonian region, $|\Delta n|$ recovered to the same level as an initial one. After the recovery, $|\Delta n|$ steeply increased at $\dot{\gamma} \simeq 1500s^{-1}$ and saturated. In Fig. 2(b), on the other hand, $|\Delta n|$ weakly increased with shear rate until $\dot{\gamma} \simeq 200s^{-1}$. Then it suddenly increased when the shear-thickening appeared and reached to the saturated value which has the same intensity as that of c = 20 wt%.

Rheo-SALS measurement clarifies that these differences

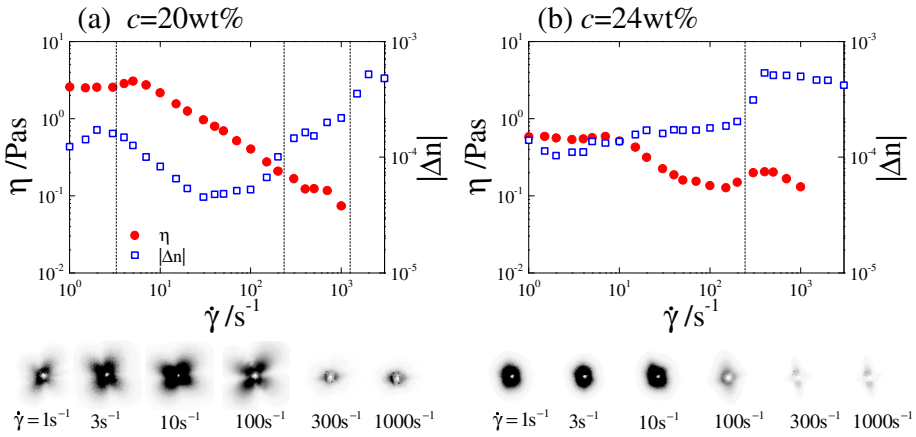

Fig. 2 Viscosity and birefringence intensity as a function of shear rate for (a): c = 20 wt% and (b): c = 24 wt%, respectively. Vertical dotted lines indicate characteristic shear rates at which the structural transitions are appeared. In the bottom, rheo-SALS patterns at several shear rates are shown. In the SALS pattern, vertical and horizontal directions correspond to the flow and neutral directions, respectively.

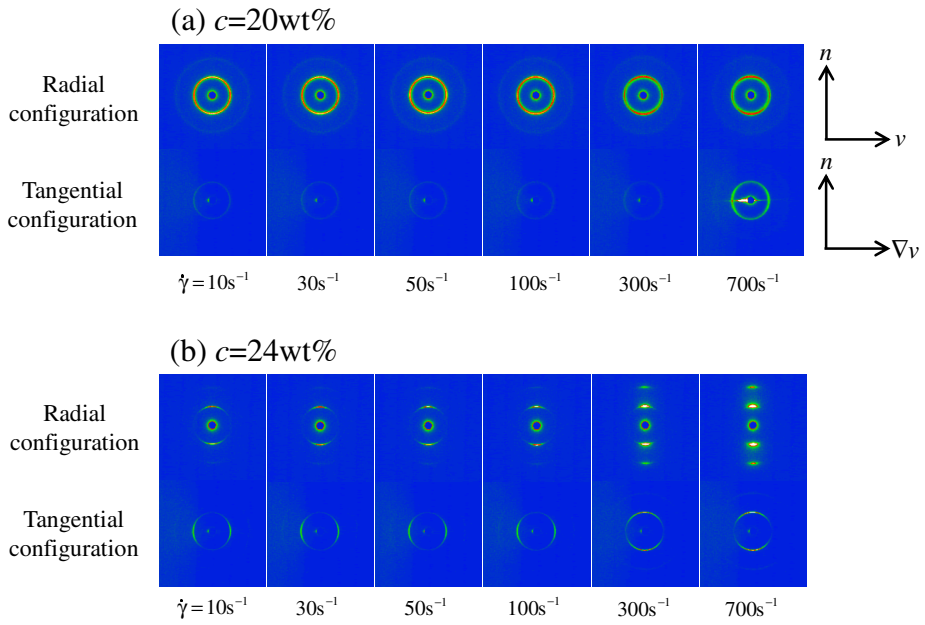

Fig. 3 Rheo-SAXS patterns at several shear rates for (a): c = 20 wt% and (b): c = 24 wt% are shown. In the radial and tangential configurations, scattering patterns in the neutral-flow plane and the neutral-velocity gradient plane are shown, respectively.

between 20 wt% and 24 wt% come from characteristic layer orientation. As shown in the bottom of Fig. 2, a four lobe cloverleaf pattern was observed at c = 20 wt%, while nothing was observed at c = 24 wt%. The four lobe pattern is a typical feature of the onion phase formation [4, 5]. The four lobe pattern first appeared when |Δn| decreased in the shear-thickening region. Pattern gradually developed with the shear rate until $\dot{\gamma} \simeq 100s^{-1}$. Onion structure is composed of spherically aligned membranes. Because of its concentrically closed layers, it is reasonable that the birefringence intensity decreased as the onion formation was induced from planar lamellar phase. The critical shear rate of the onion phase formation $\dot{\gamma}_o$ was thus determined by appearance of the shear-thickening and reduction of |Δn|. The four lobe pattern (the onion phase) disappeared when |Δn| recovered to the initial value at $\dot{\gamma} \simeq 300s^{-1}$. No characteristic scattering pattern was recognized in the high shear rate region. On the contrary to that, the sample with c = 24 wt% showed no any unique scattering patterns at low shear rate. As |Δn| was suddenly jumped up, even scattered light also disappeared.

For more detailed understanding of the layer orientation, rheo-SAXS patterns in these systems are also compared in Fig. 3. In (a), isotropic Bragg scattering was observed both in radial and tangential configurations. Isotropic pattern definitely indicates the onion phase formation because of the radial symmetry of layers in the onion structure. At $\dot{\gamma} = 300s^{-1}$ where |Δn| recovered to the initial value, the Bragg peak along the neutral direction (n) appeared in the radial configuration. And further increase in the shear rate gener-

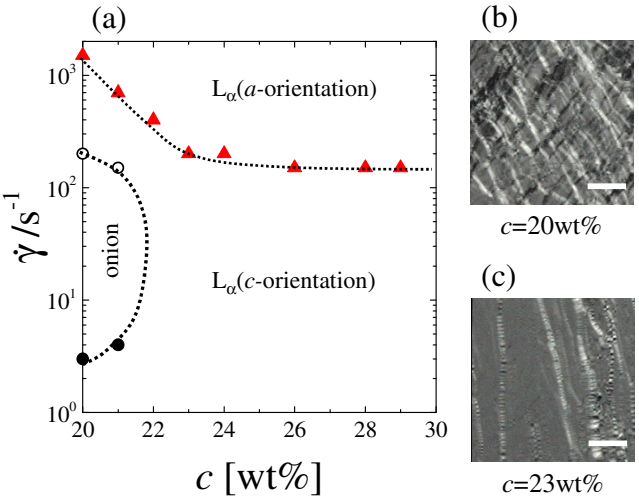

Fig. 4 (a): Dynamic orientation state as a function of shear rate and polymer concentration. Filled and open circles correspond to the critical shear rate of the onion phase formation $\dot{\gamma}_0$ and breakdown. Triangle corresponds to the critical shear rate of the layer orientation transition, $\dot{\gamma}_{c/a}$. Dotted curves are the guide for eyes. Microscopy images for (b): c = 20 wt% and (c): 23 wt% observed at $\dot{\gamma} = 1\text{s}^{-1}$ are also shown. Scale bar corresponds to 100 μm.

ated the Bragg peak along the velocity gradient direction (∇v) in the tangential configuration at $\dot{\gamma} = 700\text{s}^{-1}$. This demonstrates that the bilayers were aligned parallel to the wall of the shear cell, i.e. the onion phase was broken down and layers recovered *c*-orientation at high shear rate. Recovery of |Δn| will thus correspond to the breakdown of the onion structure and reformation of planar lamellar phase with *c*-orientation.

In (b), on the other hand, strong Bragg peak was observed in the radial and tangential configurations at lower shear rate where |Δn| showed no significant shear rate dependence. The Bragg peaks confirms the *c*-orientation. At $\dot{\gamma} = 300\text{s}^{-1}$, however, drastic change in the Bragg peak was observed. One can realize that the second Bragg peak appeared in the radial configuration, and in the tangential configuration, the Bragg peak along the neutral direction appeared but not along the gradient one. This drastic change in the Bragg peak clearly indicates that the layers reoriented from *c* to *a*-orientation. Steep increase in |Δn| can be thus identified as a unique feature of the layer orientation transition. The critical shear rate of the layer orientation $\dot{\gamma}_{c/a}$ was thus determined by the steep increase in |Δn|. We notice that the intensity of |Δn| at high shear rate is the same as that of previous experiments [4]. Rheometry and birefringence measurements were performed for other samples.

On the basis of the shear rate dependence of the viscosity and birefringence, the critical shear rates for the onion formation $\dot{\gamma}_0$ and layer orientation transition $\dot{\gamma}_{c/a}$ were respectively determined. Obtained results were summarized as a dynamic orientation diagram in Fig. 4. At low polymer concentration, the shear-induced onion phase appeared in the middle shear rate range, $3\text{s}^{-1} \le \dot{\gamma} \le 200\text{s}^{-1}$. As the polymer concentration was increased, $\dot{\gamma}_{c/a}$ steeply decreased. At higher polymer concentration region (≥ 23 wt%), the onion phase formation was never observed and $\dot{\gamma}_{c/a}$ showed almost no polymer concentration dependence. There seems be threshold concentration above which the onion phase formation is never induced.

The mechanism of the layer orientation transition in the lyotropic lamellar phase was theoretically argued by some researchers [13–15]. Ramaswamy argued that the suppression of undulations triggers the transition [13]. Lyotropic lamellar phase is stabilized by a steric repulsive force arising from undulation fluctuation [18]. As a result of the suppression of the undulation fluctuation by shear flow, reduction of the repulsive force will induce the instability. If shear stress iron out membranes, the stability of the lamellar phase will be lost and new alignment, i.e., perpendicular orientation, will be realized. In his prediction, the critical shear rate of the layer orientation transition is given by

$$\dot{\gamma}_{c/a} = \frac{(k_B T)^3}{\eta_s \kappa^2 d^3} \quad . \tag{1}$$

Here, k_B is Boltzmann's constant, T the temperature, η_s solvent viscosity, d the lamellar spacing, and κ the rigidity constant of the membranes, respectively. Validity of the theoretical prediction was experimentally confirmed for the ionic surfactant AOT lamellar phase [20]. In AOT dilute lamellar phase, the dependence of $\dot{\gamma}_{c/a}$ on layer spacing d agrees with the prediction, if the d-dependence of the zero-shear viscosity η_0 is incorporated instead of ηs. Bruinsma and Rabin also used the viscosity of the lamellar phase instead of the solvent viscosity. They estimated the critical shear rate to be a similar relation to eq. 1, although they obtained different power law exponents [21]. Since typical rigidity constant κ of the membrane is $\kappa \approx k_B T$ [19], both theoretical prediction are reduced to the form of

$$\dot{\gamma}_{c/a} \cong \frac{k_B T}{\eta_0 d^3} \quad . \tag{2}$$

Here, we assumed that the concentration dependence of the rigidity constant κ is negligible because the lamellar phase in this study was obtained within narrow concentration range.

In Fig. 5, we confirmed validity of the prediction eq. 2. For the reference, polymer concentration dependence of zero-shear viscosity η_0 and lamellar spacing d are also shown in panel (a) and (b). In Fig. 5(b), the experimental value of d reported in previous study is plotted [5]. Concentration dependence of d was well fitted by power law relation $d(\text{nm}) = 108.6 \times c^{-0.61}$. In Fig. 5(c), product of the critical shear rate and zero-shear viscosity $\dot{\gamma}_{c/a}\,\eta_0$ is plotted against d^{-3}. Value of d at each polymer concentration was estimated by interpolating into the fitted power law relation.

We first mention d^{-3}-dependency. As can be seen in Fig. 5(c), $\dot{\gamma}_{c/a}\,\eta_0$ showed two branches. In large d^{-3} region corresponding to high concentration, $\dot{\gamma}_{c/a}\,\eta_0$ increased with

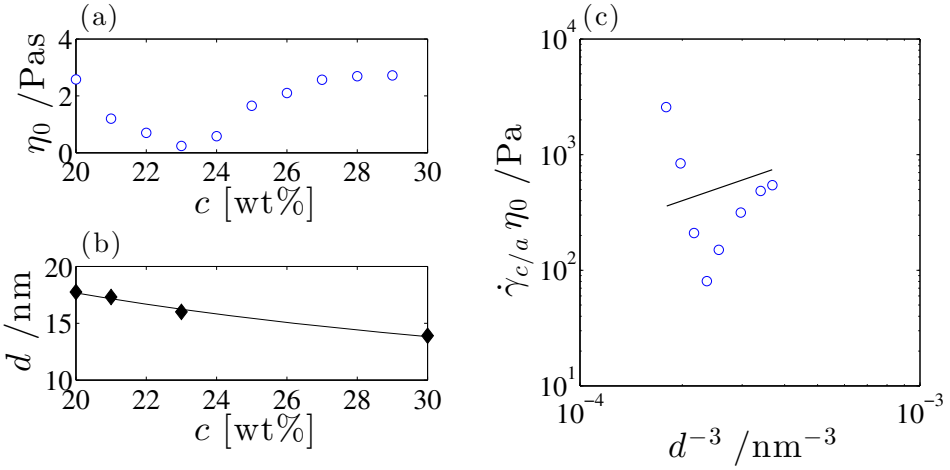

Fig. 5 Concentration dependence of (a): zero-shear viscosity η_0 and (b): the lamellar spacing d. Here, experimental value of d in ref. [5] was reproduced. Solid curve is the best fit to power law relation. (c): The product $\dot{\gamma}_{c/a}\,\eta_0$ plotted against d^{-3}. Solid line shows k_BT/d^3. Value of d at each polymer concentration was estimated by interpolating into the fitted power law relation in the panel (b).

d^{-3}. In previous study, scaling behavior predicted in eq. 2 was experimentally confirmed for dilute lamellar phase [20]. In this study, $\dot{\gamma}_{c/a}\,\eta_0$ did not show specific linearity against d^{-3}. The slope seems to approach to the unity as d^{-3} is increased. Using experimental values of η_0 and d, however, we obtain $\dot{\gamma}_{c/a} \simeq 200 - 500$ s^{-1}, which correspond to the experimental value $\dot{\gamma}_{c/a}$. k_BT/d^3 drawn as a solid line in Fig. 5(c) actually consistents with $\dot{\gamma}_{c/a}\,\eta_0$. For the comparison, we also estimated the critical shear rate by the use of the viscosity at $\dot{\gamma}_{c/a}$. Estimated value $\dot{\gamma}_{c/a} \simeq 2000 - 2500$ s^{-1} was much higher than the experimental result. Our estimation of the critical shear rate suggests that reasonable agreement with the prediction is obtained by the use of η_0. The lamellar phase in Pluronic P123 system is obtained only within narrow concentration range. In such narrow concentration (or d^{-3}) range, it will be difficult to clearly determine the slope.

Next we mention the negative slope in small d^{-3} region. Opposite result to the prediction will be attributed to essentially different mechanism from the Helfrich stabilized lamellar phase. Negative slope is observed at low polymer concentration where the formation and breakdown of the onion phase occur prior to the layer orientation transition. In order to understand "*re-orientation*" transition from lamellae to onion to lamellae, the picture of the Helfrich stabilized lamellar phase should be modified by incorporating another effect.

We previously showed that the onion phase formation is significantly mediated by defect dynamics [10]. Typical defect in the lyotropic lamellar phase is an oily steak composed of focal conic domains [23]. Our previous finding is that the onion phase formation is triggered when the density of oily streak defects anomalously increases. Actually we also confirmed that no onion phase formation is observed if anomalous increase in the defect density does not occur. The defect is essential to induce the onion phase formation. In Fig. 4, polarized microscopy images for the system with c = 20 wt% and 23 wt% at $\dot{\gamma} = 1$s^{-1} are shown. At c = 20 wt%, one can see a developed network of thin oily streaks, while only small amount of thick oily streaks can be seen at c = 23 wt%. The defective nature at low concentration is closely related to the onion phase formation. Such defective nature will be retained even after the onion phase is broken down into the planar lamellae with c-orientation. In the defective lamellar phase, shear flow easily generates more defects to relieve the imposed strain on the membranes. Therefore the instability induced by the suppression of the undulation will not occur readily. In order to allow the instability to grow up in the defective lamellar phase, the shear rate must be faster than the creation of the defect. Characteristic rate of the defect formation is determined by a mobility of dislocations [19]. Characterization of dislocations would be useful to understand the detailed mechanism of the structural transition. As an additional remark, Moreau et al. mentioned that the dislocation size is correlated with the onion phase formation and orientation transition [3] Inhibition of the layer orientation transition in the defective lamellar phase at lower concentration would be attributed to suppression of the instability due to the defect formation.

In the defective lamellar system, the stability is not simply attributed to the Helfrich interaction. Furthermore, the hydrodynamic theory based on the Helfrich Hamiltonian is broken down. It would be required to incorporate the effect of the defect generation additionally to the Helfrich interaction. Actually it has been pointed out that the critical shear rate of the onion phase formation also shows remarkable discrepancy from the theoretical prediction that only considers the Helfirch interaction [6–8, 16]. All of present issues concerning with the mechanism of the shear-induced onion phase and orientation transition seems to be attributed to the violation of the Helfrich stabilized lamellar phase due to defects.

4. Conclusion

In summary, we studied the layer orientation transition of the lyotropic triblock copolymer lamellar phase. The critical shear rate of the layer orientation transition obtained at high concentration well agrees with the theoretical prediction. On the contrary, the critical shear rate at low concentration significantly deviates from the prediction. The deviation is attributed to the violation of the Helfrich stabilized system due to the defective nature of the lamellar phase. The creation of defects by shearing will prevent the occurrence and growth of the instability.

Acknowledgements SF thanks T. Takahashi for use of the stress controlled rheometer MCR-301 equipped with a small angle light scattering and flow birefringence apparatus. SF also acknowledges support from the Grant-in-Aid for Scientific Research (B) grant No. 25287107 from the Ministry of Education, Culture, Sports, Science and Technology (MEXT) of Japan.

References

1. Diat O, Roux D, Nallet F. Effect of shear on a lyotropic lamellar phase. J Phys II France. 1993; 3: 1427.
2. Roux D, Nallet F, Diat O. Rheology of lyotropic lamellar phase. Europhys Lett. 1993; 24: 53.
3. Moreau P, Navailles L, Giermanska-Kahn J, Mondain-Monval O, Nallet F, Roux D. Dislocation-loop-mediated smectic melting. Europhys Lett. 2006; 73: 49.
4. Zipfel J, Berghausen J, Schmidt G, Lindner P, Alexandridis P, Richtering W. Influence of shear on solvated amphiphilic block copolymers with lamellar morphology. Macromolecules. 2002; 35: 4046.
5. Berghausen J, Zipfel J, Lindner P, Richtering W. Influence of water soluble polymers on the shear-induced structure formation in lyotropic lamellar phase. J Phys Chem B. 2001; 105: 11081.
6. Kosaka Y, Ito M, Kawabata Y, Kato T. Lamellar-to-onion transition with increasing temperature under shear flow in a nonionic surfactant/water system. Langmuir. 2009; 26: 3835.
7. Ito M, Kosaka Y, Kawabata Y, Kato T. Transition processes from the lamellar to the onion state with increasing temperature under shear flow in a nonionic surfactant/water system studied by rheo-SAXS. Langmuir. 2011; 27: 7409.
8. Fujii S, Richtering W. Size and viscoelasticity of spatially confined multilamellar vesicles. Eur Phys J E. 2006; 12: 269.
9. Fujii S, Mitsumasu D, Isono Y, Richtering W. Shear-induced onion formation of polymer-grafted lamellar phase. Soft Matter. 2012; 8: 5381.
10. Fujii S, Richtering W. Shear quench-induced disintegration of nonionic surfactant C10E3 onion phase. Soft Matter. 2013; 9: 5391.
11. Panizza P, Archambault P, Roux D. Effects of shear on the smectic A phase of thermotropic liquid crystals. J Phys II France. 1995; 5: 303.
12. Fujii S, Ishii Y, Komura S, Lu C-Y D. Smectic rheology close to the smectic-nematic transition. Europhys Lett. 2010; 90: 64001.
13. Ramaswamy S. Shear-induced collapse of the dilute lamellar phase. Phys Rev Lett. 1992; 69: 112.
14. Marlow S W, Olmsted P D. The effect of shear flow on the Helfrich interaction in lyotropic lamellar systems. Eur Phys J E. 2002; 8: 303.
15. Wunenburger A S, Colin A, Colin T, Roux D. Undulation instability under shear: A model to explain the different orientations of a lamellar phase under shear? Eur Phys J E. 2000; 2: 277.
16. Zilman A G, Granek R. Undulation instability of lamellar phases under shear: A mechanism for onion formation? Eur Phys J B. 1999; 11: 593.
17. de Gennes P G, Prost J. The physics of liquid crystals. London: Carendon Press; 1993.
18. Helfrich W. Steric interactions of fluid membranes in multilayer systems. Z Naturforsch. 1978; 33a: 305.
19. Oswald P, Pieranski P. Smectic and columner liquid crystals. Boca Raton: Taylor & Francis; 2006.
20. Al kahwaji A, Kellay H. Observations of the collapse of dilute lyotropic lamellar phases under shear flow. Phys Rev Lett. 2000; 84: 3073.
21. Bruinsma R, Rabin Y. Shear-flow enhancement and suppression of fluctuations in smectic liquid crystals. Phys Rev A. 1992; 45: 994.
22. Ueki T, Hiragi Y, Kataoka M, Inoko Y, Amemiya Y, Izumi Y, Tagawa H, Muroga Y. Aggregation of bovine serum albumin upon cleavage of its disulfide bonds, studied by the time- resolved small-angle x-ray scattering technique with synchrotron radiation. Bio Phys Chem. 1985; 23: 115.
23. Boltenhagen P, Lavrentvich O, Kleman M. Oily streaks and focal conic domains in Lα lyotropic liquid crystals. J Phys II France. 1991; 1: 1233.